Distortion of magnetic evoked fields and surface potentials by conductivity differences at boundaries in brain tissue

Jin-Chu Huang, Charles Nicholson, and Yoshio C. Okada
Department of Physiology and Biophysics, New York University Medical Center, New York 10016

ABSTRACT We investigated the conditions under which inhomogeneity in electrical conductivity may significantly modify the magnetic evoked field (MEF) due to primary currents (i.e., neuronal currents) in the brain. In the case of an isolated turtle cerebellum immersed in a large bath of physiological saline, our theoretical analysis showed the cerebellar surface to significantly enhance the MEF due to a primary current, by a factor of as much as two, for experimentally determined values of the conductivities of the cerebellar tissue and saline. A further parametric investigation of the conductivity effect revealed that conductivity boundaries may significantly modify the MEF due to neuronal currents located within 1 mm of a conductivity boundary, as would be the case for active neurons near an edema, an anoxic fringe such as might occur during stroke, or a ventricle in the human head. For a stationary neural source, conductivity boundaries may modify the magnitude of its MEF without affecting its temporal waveform. However, this boundary effect was found to be small for a model geometry locally approximating cortical sources in a sulcus or a fissure, where the boundary effects from adjacent sulcal walls tend to cancel each other.

INTRODUCTION

Conductivity boundaries distort the current in a volume conductor such as the human head. The magnetic field **B** and electrical potential Φ produced by a current generator in a head, assumed to be a piecewise homogeneous, isotropic conductor, are in general given by the following equations (Barr et al., 1966; Geselowitz, 1967, 1970):

$$\mathbf{B}(\mathbf{r}) = \frac{\mu_0}{4\pi} \int_V \mathbf{J}_p(\mathbf{r}') \times \nabla\left(\frac{1}{R}\right) dv' + \frac{\mu_0}{4\pi} \Delta\sigma \int_s \Phi(\mathbf{r}') \nabla\left(\frac{1}{R}\right) \times d\mathbf{S}' \quad (1a)$$

$$\Phi(\mathbf{r}) = \frac{1}{4\pi\bar{\sigma}} \int_V \mathbf{J}_p(\mathbf{r}') \cdot \nabla\left(\frac{1}{R}\right) dv' + \frac{1}{4\pi\bar{\sigma}} \Delta\sigma \int_s \Phi(\mathbf{r}') \nabla\left(\frac{1}{R}\right) \cdot d\mathbf{S}', \quad (1b)$$

where $\mathbf{r}'$ and $\mathbf{r}$ are the position vectors to the source and field points, respectively, μ_0 is the permeability of free space, $\mathbf{J}_p(\mathbf{r}')$ represents a primary current density due to current generators such as neurons in the brain, $R = |\mathbf{r}' - \mathbf{r}|$ is the distance from the volume element dv' (or surface vector element $d\mathbf{S}'$) to the field point, $\Delta\sigma = \sigma'' - \sigma'$ is the difference in conductivity at a boundary S separating a primed region from the adjacent double-primed region and $\bar{\sigma}$ is the average electrical conductivity at the field point where Φ is evaluated. The gradient operator is with respect to source points. In these equations, the first term represents the contribution by the primary source $\mathbf{J}_p(\mathbf{r}')$ and the second term the boundary effects where the integral is over the surface of each boundary in the conducting medium. Commonly, the term "secondary source" is applied to $\Delta\sigma\Phi\mathbf{n}$, where $\mathbf{n}$ is the unit vector normal to the surface S at the source point of evaluation, because the boundary effect can be considered as being due to a distributed set of dipolar current sources having moments of $\Delta\sigma\Phi$ (Geselowitz, 1967, 1970).

The second term may significantly alter the magnetic field as well as the electrical potential on the surface (e.g., scalp) of such a volume conductor. The skull has been shown to significantly modify the spatial pattern of the magnetic field outside the head when its inner surface deviates from sphericity (Stok et al., 1987; Janday and Swithenby, 1987; Hämäläinen and Sarvas, 1987, 1989; Meijs et al., 1988). Edema and regions of calcification may also distort the spatial pattern of magnetic field (Ueno et al., 1983). Other model studies have shown that the magnetic field may be modified by the interior wall of the base of skull (Iramina and Ueno, 1988) and by low and high conductivity surfaces along the midline (Cuffin, 1982, 1985; Janday and Swithenby, 1987). These results indicate that the boundary effect must be seriously reck-

---

Address correspondence to Dr. Yoshio Okada, VA/LANL/UNM Center for Magnetoencephalography, V. A. Medical Center, Albuquerque, NM 87108.

Biophys. J. © Biophysical Society
Volume 57 June 1990 1155-1166
0006-3495/90/06/1155/12 $2.00

oned with to correctly interpret the magnetic field as well as the surface potential.

This study evaluates the distortions introduced by conductivity boundaries, by manipulating the distance of a primary source from conductivity boundaries and the ratio of conductivities across such a boundary. In earlier studies (e.g., Janday and Swithenby, 1987; Hämäläinen and Sarvas, 1989; Ueno et al., 1985), this distance was generally chosen to be >1 cm, primarily for computational reasons as will be elaborated later. In contrast the present analysis focused on distances of <1 cm, mostly <1 mm, because cortical sources can be within a few hundred microns of the cerebrospinal fluid. The conductivity ratio was also varied within a physiological range, based on our experimental measurements (Okada et al., 1989) as well as on published values by other investigators (e.g., Nicholson and Rice, 1986).

The conductivity effects were initially studied to understand the magnetic evoked field (MEF) produced by an isolated turtle cerebellum immersed in a large bath of physiological saline (Okada et al., 1987; Okada and Nicholson, 1988). For the turtle cerebellum we initially found that the boundary effect was surprisingly large; the calculated magnetic field enhancement due to the boundary was in some cases much larger than the MEF due to the primary neuronal currents (Huang et al., 1989). We thus carried out a parametric analysis of the boundary effect not only for this geometry, but also for other geometries modeling cortical sources. Our results provide some new insight into the conditions in which the boundary effect may be quite important and those in which the boundary effect may be ignored in interpreting the magnetic field from the human brain.

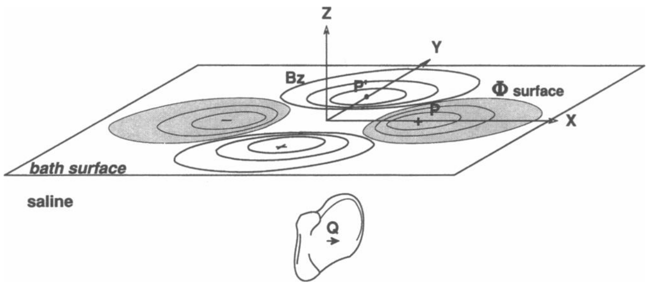

FIGURE 1 Geometry of the experimental arrangement for an isolated turtle cerebellar preparation. The primary neuronal current was modeled by a current dipole Q perpendicular to the cerebellar surface, 10 mm below the origin. The component of the magnetic field normal to bath surface (Bz) was calculated along the y-axis and the surface electric potential ($\Phi_{surface}$) along the x-axis. P and P' are the positive extremum for the $\Phi_{surface}$ and the outwardly directed field extremum of the B_z, respectively.

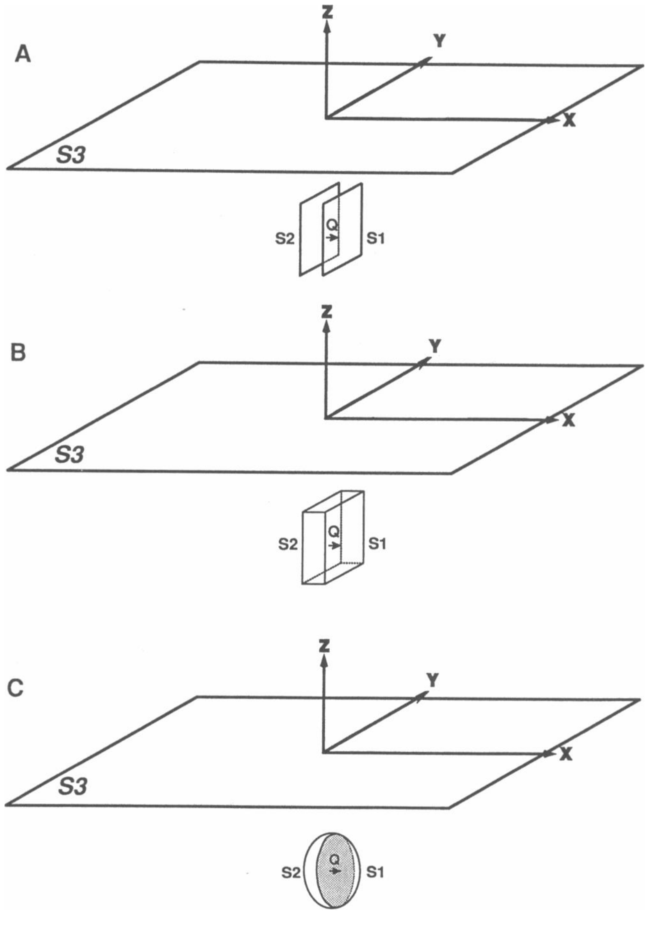

FIGURE 2 Model geometries for turtle cerebellar preparation. (A) Infinite slab of 1 mm thickness. (B) Rectangular box of $5 \times 5 \times 1$ mm. (C) Oblate spheroid of 5 mm diameter and 1 mm thickness. Equivalent primary source Q was located 10 mm below the bath surface.

METHODS

The turtle cerebellum (5 mm in diameter and 1 mm thick) was considered to be immersed vertically in a large bath of physiological saline at a depth of 10 mm (referred to the center of the cerebellum) (Fig. 1). This geometry mimicked our experimental arrangement (Okada and Nicholson, 1988). The neuronal current source evoked by an external stimulation was modeled by a single 10 nA·m current dipole (Q) placed along the center axis of the cerebellum, perpendicular to the cerebellar surface. For this geometry, we calculated the electrical potential on the bath surface ($\Phi_{surface}$) and on the cerebellar surface and the component of the magnetic field normal to bath surface (B_z) that are due to Q and those due to the distributed set of secondary sources at the boundary between the cerebellum and saline.

Three methods were used to determine Φ at the cerebellar boundary with the primary source Q located in the center of each model cerebellum (Fig. 2):

(a) *Method of images.* The cerebellum was approximated by an infinite slab of thickness $D = a + b$ (consider that a primary source Q was located at the distance of a from surface S_1 and b from surface S_2) and conductivity σ_{in} immersed in physiological saline of conductivity σ_{out} (Fig. 2 A). As described in the next section, the potential Φ on both surfaces of the slab could be found from an analytical equation that related Φ to the sum of potentials due to all the images of **Q**.

(*b*) *Method of integral equation (boundary element method)*. The cerebellum was represented by a rectangular box of 5 × 5 mm in surface dimension and 1 mm in thickness, having a conductivity σ_{in}. This was immersed in a saline of conductivity σ_{out} (Fig. 2 *B*). The potential Φ on the cerebellar surfaces S_1 and S_2 and on the bath surface S_3 were found from Fredholm's integral equation described in the next section.

(*c*) *Method of Poisson equation*. The cerebellum was represented by an oblate spheroid, 5 mm in diameter along its major axis and 1 mm along its minor axis, with a conductivity of σ_{in}. This was immersed in saline of conductivity σ_{out} (Fig. 2 *C*). The potential Φ on the cerebellar surface was found from the analytical solution of the Poisson equation subjected to the boundary conditions for an oblate spheroid immersed in a homogeneous conducting medium as described in the next section.

In solving the integral equation, we considered two cases. In the first case, we included the bath surface S_3 as well as surfaces S_1 and S_2 (Fig. 2 *B*), ignoring the surfaces on the four sides of the rectangular box. The surfaces on the sides of the box did not contribute significantly to the potential on the large surfaces S_1 and S_2 because the rectangular box was relatively large compared to its thickness. The numerical results showed that the maximum potential on the bath surface was, for the ratio of conductivity used in our present analysis, at least three orders of magnitude smaller than the maximum potential on the cerebellar surface. Thus, S_3 could be ignored in comparing the potential on the cerebellar surface calculated with the boundary element method to those obtained from the methods of images and Poisson equation (see Fig. 5).

The analytical equations for the three methods enabled us to calculate Φ on the surfaces of the model cerebellum, assuming it was immersed in an infinite homogeous volume conductor. Once Φ was found, Eq. 1 could be applied to find **B** and $\Phi_{surface}$. In the integrand, $\mathbf{J}_p$ was replaced by **Q** times a delta function, $\mathbf{J}_p(\mathbf{r}) = \mathbf{Q}\,\delta(\mathbf{r} - \mathbf{r}_o)$, where the current dipole **Q** was at the location $\mathbf{r}_o$.

The comparison of results from these three methods enabled us to validate our analytical and numerical solutions. Once these methods were cross-validated, $\Phi_{surface}$ and B_z were calculated from the computed values of Φ, using the integral equation method.

In addition to the turtle cerebellum, the boundary effect was studied in other conductivity geometries to gain a wider picture of this important effect. One geometry modeled a neural source located at a varying distance from a region of differing conductivity. The second geometry mimicked a cortical neuronal source located in one side of a sulcus or a fissure.

THEORETICAL RESULTS

1. Method of images

Consider that a primary source **Q** is located in an infinite slab of conductivity σ_{in} at the distance of a from surface S_1 and b from surface S_2 (Fig. 3). These two surfaces produce an infinite number of pairs of images along the axis of symmetry. Each pair of images are characterized by the following formula:

$$Q_m = \left(\frac{\sigma_{out} - \sigma_{in}}{\sigma_{out} + \sigma_{in}}\right)^m Q = \left(\frac{\Delta\sigma}{2\bar{\sigma}}\right)^m Q, \qquad (2)$$

where m is the order of the image. Note that this equation reduces to $Q_m = Q$ when $m = 0$. Thus, when $\sigma_{in} < \sigma_{out}$ (Fig. 3 *a*), the image dipoles will have the same orientation as the primary source. But, when $\sigma_{in} > \sigma_{out}$, their directions alternate as indicated in Fig. 3 *b*.

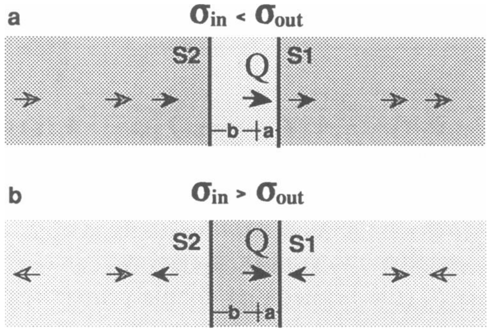

FIGURE 3 Images of the primary source **Q** in an infinite slab of thickness $a + b$ immersed in an infinite homogeneous volume conductor. Image pairs up to the third order are shown in pairs (by arrows with lighter arrowheads) for two ratios of conductivity. The magnitudes of the secondary sources are not correctly indicated here. Note also that **Q** was 0.3 mm for S_2 in the calculations for Fig. 5, unlike this arbitrary example.

The potential Φ_{prim} on S_1 due to the primary source alone is given by:

$$\Phi_{prim} = \frac{Q}{4\pi\sigma_{in}} \frac{\cos\theta}{a^2 + y^2 + z^2}, \qquad (3)$$

where y and z are the coordinates on the S_1 plane, θ is the angle between the current dipole and the position vector for the field point.

The total potential on S_1 due to both the primary source and images for a general asymmetric case is given as:

$$\Phi = \frac{Q}{4\pi\bar{\sigma}} \sum_{n=0}^{\infty} \left(\frac{\Delta\sigma}{2\bar{\sigma}}\right)^{2n} \frac{\cos\theta}{[2nb + (2n+1)a]^2 + y^2 + z^2} + \frac{Q}{4\pi\bar{\sigma}} \sum_{n=1}^{\infty} \left(\frac{\Delta\sigma}{2\bar{\sigma}}\right)^{2n-1} \frac{\cos\theta}{[2nb + (2n-1)a]^2 + y^2 + z^2}, \qquad (4)$$

where a and b are defined as in Fig. 3 (see Appendix for the derivation). Note that $\Phi = \Phi_{prim}$ when $\sigma_{in} = \sigma_{out}$ as it should be when there is no conductivity boundary, $\Phi = 2\Phi_{prim}$ as it should be for a semiinfinite volume conductor when $\sigma_{out} = 0$ and b is large. When the primary source is in the middle of the slab ($a = b$), the potential Φ on S_1 due to the primary source and the images can be found from a special case of Eq. 4 as:

$$\Phi = \frac{Q}{4\pi\bar{\sigma}} \sum_{n=0}^{\infty} \left(\frac{\Delta\sigma}{2\bar{\sigma}}\right)^{n} \frac{\cos\theta}{[(2n+1)a]^2 + y^2 + z^2}. \qquad (5)$$

2. Boundary element method

The distribution of Φ on the rectangular boundary surfaces was obtained by solving the Fredholm's equation

(Barnard et al., 1967*a* and *b*; Lynn and Timlake, 1968*a* and *b*):

$$\Phi_{\mathrm{k}}(\mathbf{r}) = \frac{\sigma_{\mathrm{s}}}{\overline{\sigma}_{\mathrm{k}}}\Phi_{\infty}(\mathbf{r}) - \frac{1}{4\pi\overline{\sigma}_{\mathrm{k}}}\sum_{\mathrm{j}}^{N}\Delta\sigma_{\mathrm{j}}\int\Phi_{\mathrm{j}}(\mathbf{r}')\,\mathrm{d}\Omega_{\mathrm{kj}} \quad (6)$$

where Φ_{∞} is the potential produced by the primary source only, σ_{s} is the conductivity in the source region, $\overline{\sigma}_{\mathrm{k}}$ is the average conductivity at the boundary S_{k}, $\Delta\sigma_{\mathrm{j}} = \sigma'' - \sigma'$ on boundary S_{j} (the primed and double-primed regions are the cerebellum and saline, respectively, when S_{j} is the cerebellar surface and they are the saline and air regions, respectively, when S_{j} is the bath surface), and $\mathrm{d}\Omega_{\mathrm{kj}}$ is the solid angle of the surface element on S_{j} seen from a point of observation on the surface S_{k}, i.e.,

$$\mathrm{d}\Omega_{\mathrm{kj}} = \frac{(\mathbf{r} - \mathbf{r}')}{|\mathbf{r} - \mathbf{r}'|^{3}}\cdot\mathbf{n}\,\mathrm{d}S_{\mathrm{j}}, \quad (7)$$

where n is directed from the primed to the double-primed regions at surface S_{j}, $\mathbf{r}'$, and $\mathbf{r}$ are the position vectors from the origin to the source and field point, respectively.

The theoretical results in this section are not new, but we consider here the aspects of this equation that are unique to our rectangular box geometry. First, note that the potential on a flat surface S_{k} is due to the primary source plus the secondary sources on the other surfaces, excluding the surface S_{k} itself, because the solid angle equals zero when j = k. To solve the integral equations numerically, the surface S_{k} was divided into N elements $\Delta_i^{(\mathrm{k})}$ ($i = 1, 2, \ldots, N$), resulting in a set of linear equations which could be described by the matrix expression

$$\mathbf{\Phi} = \mathbf{G} + \mathbf{D}\,\mathbf{\Phi}. \quad (8)$$

The elements of matrix $\mathbf{\Phi}$, $\mathbf{G}$, and $\mathbf{D}$ were defined as:

$$\phi_i^{(\mathrm{k})} = \frac{1}{a_i^{(\mathrm{k})}}\int_{\Delta_i^{(\mathrm{k})}}\phi(\mathbf{r})\,\mathrm{d}S(\mathbf{r}),$$

$$g_i^{(\mathrm{k})} = \frac{1}{a_i^{(\mathrm{k})}}\int_{\Delta_i^{(\mathrm{k})}}G(\mathbf{r})\,\mathrm{d}S(\mathbf{r}),$$

$$\mathrm{d}_{im}^{(\mathrm{k})n} = \frac{1}{a_i^{(\mathrm{k})}}\frac{\Delta\sigma_n}{\overline{\sigma}_{\mathrm{k}}}\int_{\Delta_i^{(\mathrm{k})}}\Omega_{\Delta_m^{(n)}}(\mathbf{r})\,\mathrm{d}S(\mathbf{r}), \quad (9)$$

where $a_i^{(\mathrm{k})}$ was the area of the ith element $\Delta_i^{(\mathrm{k})}$ on surface S_{k} and $\Omega_{\Delta_m^{(n)}}(\mathbf{r})$ was the solid angle subtended by $\Delta_m^{(n)}$ at $\mathbf{r}'$ viewed from point i on surface S_{k}.

The solution of the set of linear equations (Eq. 8) for our problem was stable, because a deflation technique could be used to circumvent the problem of singularity in the matrix of equations that arises when the conductivity is zero in some region (Lynn and Timlake, 1968*b*). To investigate the stability and convergence, it was solved numerically for Φ by utilizing Jacobi's iterative algorithm. Initially, we let the G (matrix) term as the zeroth-order approximation of the solution (the potential due to the primary source only without any boundary effect) and substituted the zeroth-order solution of Φ (column vector) into the right-hand side of Eq. 8 to evaluate the first-order approximation of Φ. Then we found the second-order approximation of Φ from the first-order solution, and so on. This procedure was iteratively continued until the required accuracy was achieved. Because the procedure converges, the discrepancy between two adjacent order solutions can be made as small as desired. The total number of surface elements was chosen to be 200 to 3,200 depending on the distance of the primary source **Q** from a boundary surface and the size of the surface. The size of surface element was typically ~0.25 × 0.25 mm.

It is useful to visualize the secondary sources set up at each boundary in different conditions. Fig. 4 illustrates three cases for a rectangular box. When there is no conductivity difference between the cerebellum (or any other tissue) and saline, there is of course no secondary source (Fig. 4 *A*). When the outside conductivity is lower than the tissue (Fig. 4 *B*), the secondary sources are directed opposite to the primary source. This type of boundary attenuates the external magnetic and electric signals due to the primary source. When the conductivity is higher in the saline than in the tissue (Fig. 4 *B*), the secondary sources are oriented in the same way as the primary source, thereby enhancing the electric and magnetic signals due to the primary source. The magnitude of the boundary effect is determined by the difference in conductivity and the potential Φ on each surface.

3. Method of Poisson equation

For the third method, a closed analytical solution to the Poisson equation was obtained for an oblate spheroid embedded in an infinite conducting medium with the primary source represented by a current dipole **Q** (cf. Smythe, 1968, for the general technique). That is, we

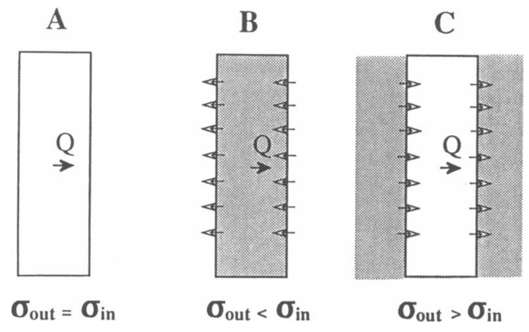

FIGURE 4 Illustration of secondary sources set up at the boundary of the model cerebellar surface for three ratios of conductivity.

solved the following Poisson equation:

$\nabla^2\Phi = -\dfrac{\rho}{\sigma_{\text{in}}}$, with boundary conditions

$$\Phi_{\text{in}} = \Phi_{\text{out}},\ \sigma_{\text{in}}\frac{\partial\Phi_{\text{in}}}{\partial n} = \sigma_{\text{out}}\frac{\partial\Phi_{\text{out}}}{\partial n}, \quad (10)$$

where ρ is the monopole source density.

The oblate spheroid is generated by rotating an ellipse around its minor axis. The equation of the spheroid is:

$$\frac{z^2}{\zeta^2} + \frac{x^2}{\zeta^2+1} + \frac{y^2}{\zeta^2+1} = c^2 \quad \zeta \geq 0, \quad (11)$$

and that of the hyperboloid is:

$$\frac{z^2}{-\xi^2} + \frac{x^2}{1-\xi^2} + \frac{y^2}{1-\xi^2} = c^2 \quad -1 < \xi < 1. \quad (12)$$

In terms of the oblate spheroidal coordinate system (ξ, ζ, ϕ), the Poisson equation becomes:

$$\frac{\partial}{\partial\xi}\left[(1-\xi^2)\frac{\partial\Phi}{\partial\xi}\right] + \frac{\partial}{\partial\zeta}\left[(1+\zeta^2)\frac{\partial\Phi}{\partial\zeta}\right] + \frac{\xi^2+\zeta^2}{(1-\xi^2)+(1+\zeta^2)}\frac{\partial^2\Phi}{\partial\phi^2} = -\frac{\rho}{\sigma_{\text{in}}}. \quad (13)$$

The coordinate transformation between the rectangular and spheroidal coordinate systems is given by:

$$\begin{aligned} x &= c\,(1-\xi^2)^{1/2}(1+\zeta^2)^{1/2}\cos\phi, \\ y &= c\,(1-\xi^2)^{1/2}(1+\zeta^2)^{1/2}\sin\phi, \\ z &= c\,\xi\,\zeta, \end{aligned} \quad (14)$$

where $c^2 = a^2 - b^2$ is the eccentricity (a and b are the major and minor axes of the spheroid).

The potential due to a current dipole $\mathbf{Q}$ can be written as $\mathbf{Q}\cdot\nabla_0\Phi$, where Φ is the potential due to a unit monopole source at the location ξ_0, ζ_0, ϕ_0, and ∇_0 denotes the gradient with respect to ξ_0, ζ_0, ϕ_0 (Berry, 1956). The total potential can be considered as the summation of the potential due to the primary source (Φ_{prim}) and the secondary source (Φ_{sec}) caused by the conductivity discontinuity at the spheroidal surface. In the inner region, the potential due to the primary and secondary sources are, respectively, given as follows:

$$\Phi_{\text{prim}} = \frac{Q}{4\pi\sigma_{\text{in}}}\frac{1}{c}\sum_{n=0}^{\infty} j\,(2n+1)Q_n(j\zeta)P_n(\xi)\hat{\mathbf{p}} \cdot \nabla_0[P_n(j\zeta_0)P_n(\xi_0)], \quad (\zeta 0 < \zeta < \zeta a) \quad (15)$$

$$\Phi_{\text{sec}} = \frac{Q}{4\pi\sigma_{\text{in}}}\frac{1}{c}\sum_{n=0}^{\infty} j\,A_n\,(2n+1)P_n(j\zeta)P_n(\xi)\hat{\mathbf{p}} \cdot \nabla_0[P_n(j\zeta_0)P_n(\xi_0)], \quad (\zeta 0 < \zeta < \zeta a) \quad (16)$$

where ξ_0, ζ_0 refer to the location of the current dipole, while ξ, ζ_a refer to the locations on the surface of the spheroid, $\hat{\mathbf{p}}$ is the unit vector of the current dipole, j is the imaginary unit, and P_n and Q_n are the associated Legendre functions of the first and second kind with real or imaginary arguments. In the outer region, the potential due to the primary and secondary sources are, respectively, given as:

$$\Phi_{\text{prim}} = \frac{Q}{4\pi\sigma_{\text{out}}}\frac{1}{c}\sum_{n=0}^{\infty} j\,(2n+1)Q_n(j\zeta)P_n(\xi)\hat{\mathbf{p}} \cdot \nabla_0[Q_n(j\zeta_0)P_n(\xi_0)], \quad (\zeta > \zeta a) \quad (17)$$

$$\Phi_{\text{sec}} = \frac{Q}{4\pi\sigma_{\text{out}}}\frac{1}{c}\sum_{n=0}^{\infty} j\,B_n\,(2n+1)Q_n(j\zeta)P_n(\xi)\hat{\mathbf{p}} \cdot \nabla_0[Q_n(j\zeta_0)P_n(\xi_0)]. \quad (\zeta > \zeta a) \quad (18)$$

Using the boundary conditions, one can find the coefficients A_n in Eq. 16 and B_n in Eq. 18. We can show that the resulting potential on the boundary of the oblate spheroid is:

$$\Phi_{\zeta_a} = -\frac{1}{4\pi\sigma_{\text{in}}}\frac{1}{c^2}\sum_{n=0}^{\infty} j\,(-1)^n(2n+1) \cdot \left[Q_n(j\zeta_a) + \frac{(\sigma_{\text{in}}-\sigma_{\text{out}})\,Q_n(j\zeta_a)P_n(j\zeta_a)}{\sigma_{\text{out}}P_n(j\zeta_a) - \sigma_{\text{in}}\dfrac{P_n'(j\zeta_a)}{Q_n'(j\zeta_a)}Q_n(j\zeta_a)}\right] \cdot P_n(j\xi)P_n'(j\zeta_0), \quad (19)$$

where the prime denotes the derivative with respect to ξ_0 and ζ_0. The first term in the bracket represents the contribution from the primary source and the second term represents the contribution from the secondary sources on the spheroidal boundary. The second term vanishes when $\sigma_{\text{in}} = \sigma_{\text{out}}$. This solution reduces to the equation given by Berry (1956) for the case $\sigma_{\text{out}} = 0$ and $\sigma_{\text{in}} = 1$, that is for the case of a spheroidal conductor surrounded by a nonconducting medium, such as air:

$$\Phi_{\zeta_a} = -\frac{1}{4\pi}\frac{1}{c^2}\sum_{n=0}^{\infty} j\,(-1)^n(2n+1) \cdot \left[Q_n(j\zeta_a) - \frac{(Q_n'(j\zeta_a)}{P_n'(j\zeta_a)}P_n(j\zeta_a)\right] \cdot P_n(\xi)P_n'(j\zeta_0). \quad (20)$$

Eq. 19 can be used to find the analytical expression for the magnetic field outside the spheroid in a manner analogous to the equation given by Cuffin (1977) for the special case of $\sigma_{\text{out}} = 0$.

NUMERICAL RESULTS

1. Electrical potential on boundary surfaces

Fig. 5 shows the potential on the cerebellar surface along a line passing through its extremum (cf. Fig. 2) on surface S_1 for a current dipole located at 0.3 mm from S_2 ($b = 0.3$

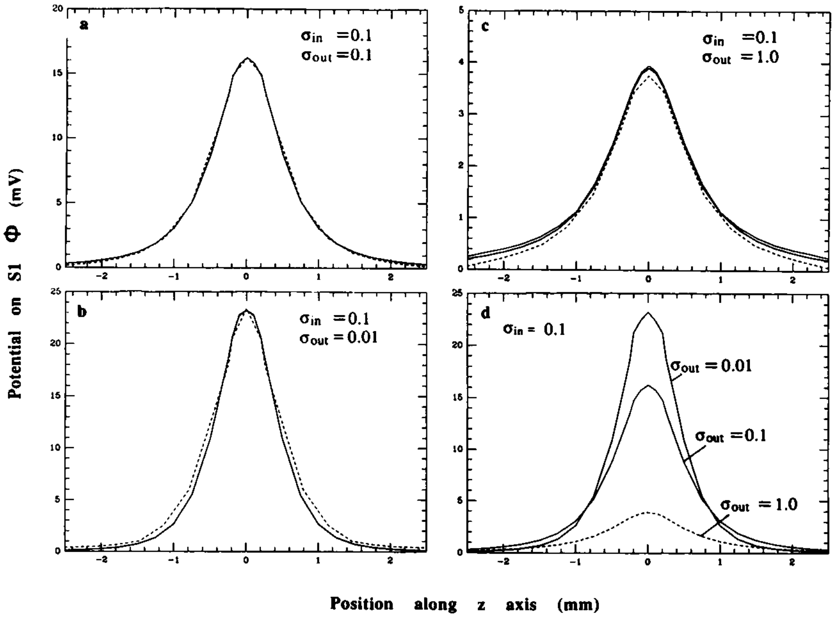

FIGURE 5 Potential profiles along a lihne on S_1 passing through the potential extremum of each model cerebellum, calculated with the method of images (*thin solid line*), the boundary element method (*thick solid line*), and the method of Poisson equation (*dashed line*). (*a*) Φ for the homogeneous case. (*b*) Φ for a highly conducting surround. (*c*) Φ for a poorly conducting surround. (*d*) Φ profile for three ratios of conductivity, calculated with the boundary element method. Q at 0.2 mm from the center toward S_1 in 1-mm-thick model cerebella.

mm in Fig. 3. The potential profiles were calculated with the three different methods. In the case of the oblate spheroid, the abscissa is the arc distance from the potential extremum on the spheroidal surface. The potential profiles were calculated for three conditions defined by $\sigma_{\text{out}} = 0.1$, 0.01, and 1.0 S/m with $\sigma_{\text{in}} = 0.1$ S/m (Fig. 5, *a–c*).

In applying Eq. 4, it was necessary to include up to the tenth-order images to obtain a convergence to <0.1% of error. While, nine iterations were needed to compute potential with the same accuracy for the second method (Eq. 6). As for Eq. 19, the computation of all Legendre functions of the first and second kind were based on recurrence relations (Abramowitz and Stegun, 1972). For function Q_n, when the magnitude of argument was <1.5, the summation converged slowly and it was necessary to keep more than 20 terms in the summation to get the same accuracy as the other methods.

The agreement is quite good among the three methods. The potential Φ calculated at the extremum on S_1 was 16.24, 16.24, and 16.21 mV for the methods of image, integral equation and Poisson equation, respectively, for the case $\sigma_{\text{in}} = \sigma_{\text{out}} = 0.1$ S/m. The small discrepancies that are evident for the other two conditions ($\sigma_{\text{in}} \neq \sigma_{\text{out}}$; Fig. 5, *b* and *c*) can be explained by differences in the geometry of the model cerebella. As mentioned earlier, the potential on a given surface (e.g., S_1) is due to the primary source and the secondary sources on the other surfaces, not including the given surface itself, when it is flat. When the surface is curved, as in a spheroid, the potential at a given point on a surface is affected by the secondary sources on the same surface. The discrepancies between the spheroid and the other two geometries are mostly due to this additional effect. This degree of agreement among three methods showed that the cerebellum was sufficiently thin and flat that it could be accurately modeled by a slab, a rectangular box, or an oblate spheroid. Moreover, this result demonstrates that the numerical methods as well as the analytical formulas we derived were correct.

Fig. 5 *d* shows the effect of varying the conductivity of the volume conductor relative to the model cerebellum (rectangular box) of conductivity $\sigma_{\text{in}} = 0.1$ S/m. The potential on surface S_1 is larger when $\sigma_{\text{in}} > \sigma_{\text{out}}$ (0.1 vs. 0.01 S/m) and lower when $\sigma_{\text{in}} < \sigma_{\text{out}}$ (0.1 vs. 1.0 S/m), in comparison with the homogeneous case. The potential declines rapidly away from the extremum, the relative fall-off being sharper when $\sigma_{\text{out}}/\sigma_{\text{in}}$ is lower.

2. External magnetic field due to primary and secondary sources

The boundary effect on the magnetic field at bath surface is illustrated in Fig. 6 for the rectangular box of conductivity $\sigma_{\text{in}} = 0.1$ S/m with a primary source in the middle of

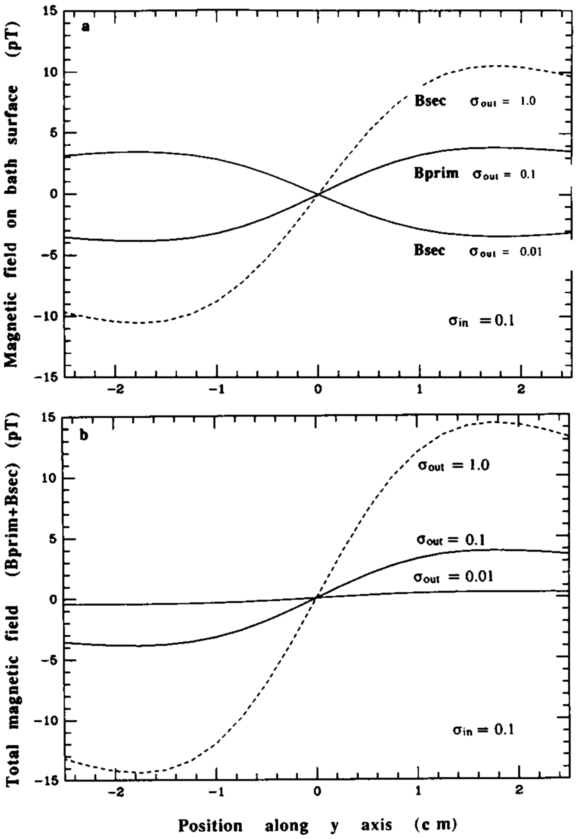

FIGURE 6 One-dimensional profile of the magnetic field (B_z) along the y-axis on bath surface. (a) Comparison of the magnetic fields due to the primary source (10 nA · m current dipole) and secondary sources. $B_{prim} = B_z$ in the homogeneous case. $B_{sec} = B_z$ inhomogeneous case due to the secondary source line. (b) Comparison of the total magnetic field in the homogeneous and inhomogeneous cases. Calculations based on the boundary element method for a rectangular box model cerebellum.

the box. These results were obtained with the boundary element method, taking into account the bath surface (S_3) as well as the cerebellar surfaces (S_1 and S_2). When σ_{out} = 1.0 S/m, the secondary source produced the magnetic field in the same direction as that of the primary source. The magnitude of the normal component of the magnetic fields due to the secondary source (B_{sec}) was nearly twice as much as that of the primary source (B_{prim}) (Fig. 6 a), so the sum of their magnetic fields was enhanced by a factor of about three (Fig. 6 b). The magnitudes were 0.39 pT for the contribution due to the primary source located in the center of the box and 0.87 pT for the contribution due to the boundaries (S_1 and S_2 together), for experimentally determined values of σ_{in} = 0.20 S/m and σ_{out} = 1.33 S/m for the turtle cerebellum and the physiological saline (Okada et al., 1989). When σ_{out} = 0.01 S/m, the B_{sec} was opposite to the B_{prim} but their magnitudes were comparable (Fig. 6 a). The resulting sum of their magnetic fields was, therefore, quite flat (Fig. 6 b). The results clearly show that the secondary sources may produce magnetic fields that are larger than those due to the primary source.

The results for the surface potential are identical to the above results for the magnetic field on bath surface. That is, the ratio Φ_{sec}/Φ_{prim} along the x-axis on the surface of the bath varies in the same way as B_{sec}/B_{prim} as a function of the conductivity ratio, when Φ_{prim} and Φ_{sec} are defined as the potentials due to the first and second terms of Eq. 1.

A further parametric analysis showed that the critical variable for this boundary effect was σ_{out}/σ_{in}. The magnetic field B_{sec} normalized with respect to the B_{prim} alone is a function of σ_{out}/σ_{in}. This ratio B_{sec}/B_{prim} is independent of individual magnitudes of σ_{out} and σ_{in}, as can be seen from the analytical equations of the previous section. The semilogarithmic diagram of Fig. 7 shows that the effect of the secondary source reaches an asymptotic value of -1.0, completely cancelling the magnetic field due to the primary source, as the conductivity of the surrounding medium approaches zero. On the other hand, when the outer conductivity becomes higher relative to that of the tissue, the magnetic field due to the secondary sources enhances the field due to the primary source without a clear asymptote within the range of our investigation. This parametric relation also holds for the surface potential.

3. Magnetic field distortion due to one boundary

Implications of the strong boundary effect found above were investigated for interpreting the magnetic field produced by the human brain. To generalize the above

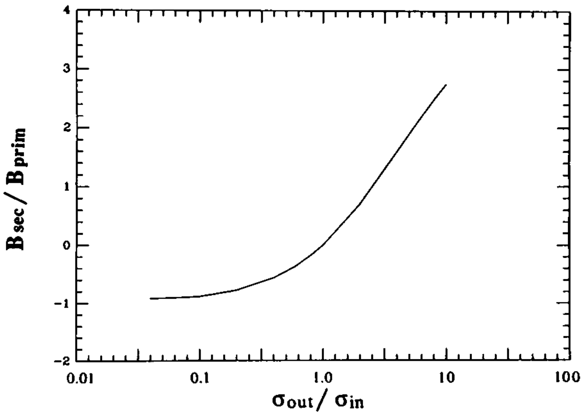

FIGURE 7 Ratio B_{sec}/B_{prim} as a function of σ_{out}/σ_{in} at the field extremum P', calculated with the boundary element method for the rectangular box model cerebellum.

result, two geometries were considered: First, as shown in the inset to Fig. 8, we studied how the boundary effect was related to the distance of a primary current to a single boundary such as one pial surface. The large effect of the secondary source for the turtle cerebellum was due in part to the presence of a second surface close (1 mm away) to the first. This interaction was eliminated and the boundary effect was evaluated for the case that is purely due to the proximity of a primary source to a single boundary. In this calculation the primary source (a current dipole Q) was located 10 mm below the top boundary. The boundary element method was applied to this geometry with the conductivity of the source region (σ_{in}) set to 0.1 S/m and the conductivity of the adjacent region (σ_{out}) set to 0.01 or 1.0 S/m. The conductivity of air above the top boundary was of course zero. The number of boundary elements on S_1, having a dimension of 10 × 10 mm, was varied between 10 × 10 (surface element = 1.0 × 1.0 mm) and 40 × 40 (surface element = 0.25 × 0.25 mm) to ascertain that the grid size was sufficiently small even at a primary source-S_1 distance of 0.1 mm.

It was found that the magnetic field due to the secondary source was larger than that for the primary source when the primary source was within 0.2 mm of the boundary. The boundary effect was equally strong for the case when a tissue with a conductivity of 0.1 S/m was adjacent to a highly conducting medium (e.g., cerebrospinal fluid) with a conductivity of 1.0 S/m and for the case where it was next to a poorly conducting medium with a conductivity of 0.01 S/m (Fig. 8). The contribution of the secondary sources was substantial for sources located within a few millimeters of the boundary (~40% at 2 mm). As in the case of Fig. 7, this boundary effect was a function of σ_{out}/σ_{in}, the effects being mirror images when the ratios were the reciprocals of each other. This result should be relevant for realistic physiological situations, because neuronal sources can be within a few millimeters of a conductivity boundary such as an edema where the conductivity should be higher, or an anoxic boundary where the conductivity should be lower than the conductivity of the normal tissue. The conductivity ratios of 0.1–10 are within a physiological range (Nicholson and Rice, 1986; Hansen, 1985).

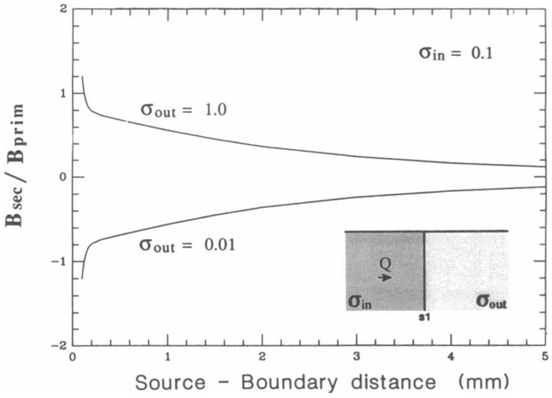

FIGURE 8 B_{sec}/B_{prim} at the field extremum P' on bath surface as a function of the distance of the primary source **Q** from a boundary S_1 separating two regions of conductivities σ_{in} and σ_{out}.

4. Magnetic field due to cortical sources in sulci and fissures

The large effects of conductivity boundaries are quite disturbing for those interested in inferring properties of the human brain based on noninvasive measurements of the extracranial magnetic field. The following results show, however, that the secondary effects at a sulcus or a fissure can be ignored when interpreting the magnetic field from cortical sources.

The sulcal area of the cortex is filled with cerebral spinal fluid in a thin space of less than a few millimeters (Gyldensted and Kostlejanetz, 1975). Thus, the secondary sources on one side of a sulcus may cancel those in the opposite side. We modeled this situation by a primary source in a tissue of conductivity 0.1 S/m next to a sulcus of conductivity 1.0 S/m (see inset of Fig. 9). The distance of the primary source to one sulcal wall was fixed at 0.5 mm and the second sulcal wall was moved away from the first wall. The boundary element method was again used to calculate the normal component (B_z) of the magnetic field at the top boundary.

As shown in Fig. 9, one wall of the sulcus reduced the boundary effect of the other wall. When two surfaces were very close, the secondary sources on the boundary surfaces had the same magnitude but opposite sign, so they canceled each other. When one surface was far away, the secondary sources on that surface became smaller, the net effect being similar to the case of a single surface as in Fig. 8, so the curve reached an asymptotic value determined by the distance of the primary source to the nearest boundary surface and the conductivity ratio at the boundary.

DISCUSSION

The above theoretical analysis provides an insight not only into the boundary effects for a turtle cerebellum, but also for more general situations that are applicable to interpreting magnetoencephalograms from the human brain. In this analysis we concentrated on the boundary effects due to primary sources located quite close to surfaces delimiting regions of differing electrical conductivities. The ratio of conductivities across several types of

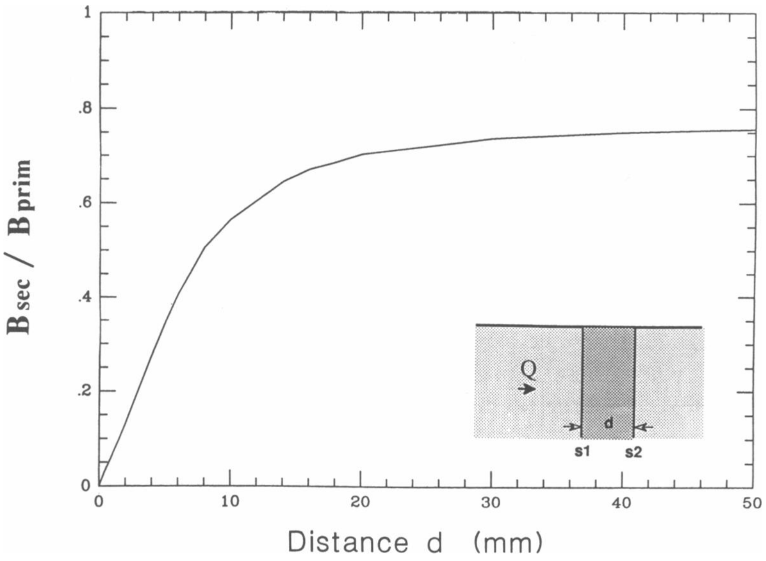

FIGURE 9 B_{sec}/B_{prim} at the field extremum P' on bath surface as a function of width d of a region with conductivity $\sigma = 1.0$ S/m embedded in a region with conductivity of 0.1 S/m. Q of 10 nA · m was located at 0.5 mm from S_1 and 10 mm below bath surface.

boundaries was chosen within a range of values known to exist in the head. In previous investigations the boundary-to-source distance was chosen to be rather large, >1 cm. This choice was forced by the constraints in the numerical techniques used to solve the potential and magnetic field problems. The numerical technique based on the boundary element method requires that each surface be divided into boundary surface elements. The size of surface elements is determined by the distance between the primary source and the boundaries as well as conductivity ratios across the boundaries. As shown in Fig. 5, the potential on one surface declined rapidly away from the potential extremum, reaching half the maximum amplitude within 0.5 mm of the distance on either side of the extremum when the source was 0.7 mm from the surface. In this case we found that it was necessary to choose surface elements having dimensions of 0.125 × 0.125 mm to obtain adequate convergence of the numerical solutions. When the entire head is modeled as a volume conductor, as in the earlier investigations, the number of surface elements can become unwieldy unless the primary source is kept away from its closest boundary. In one study, for example, (Meijs et al., 1987) the total number of surface elements was 1,280 with a distance of 2.5 cm between the primary source modeling a cortical source and the scalp surface.

In our study this problem was circumvented by choosing simple geometries and in some cases by calculating the boundary effects over a local region. We feel that this approach is justified because the boundary effects are mostly constrained within such local regions when the primary source is quite close to the boundaries as in our case.

The turtle cerebellum enabled us to study the boundary effect using three independent methods for the purpose of cross validation. Prior to our calculations, we expected the magnetic field due to the boundaries to be a fraction of the field due to the primary source. Having obtained the unexpectedly large boundary effect based on the boundary element method, this result was verified with the other independent methods. The shape of the turtle cerebellum enabled us to model it as a slab or an oblate spheroid as well as a rectangular box and, thus, it was possible to develop the analytical and numerical solutions for the methods of images and the Poisson equation.

The strong boundary effect is due to the proximity of the primary source to a boundary as well as to the relatively high conductivity ratio across the boundary. As shown in Fig. 8, the magnetic field due to the boundary increased rapidly as the primary source approached within 0.5 mm of the boundary. This effect is enhanced by adjacent surfaces when the primary source is embedded in a small active tissue surrounded by a region of differing conductivity.

The conductivity ratio of 0.1 to 10 is within the physiological range. For example, the ratio between the extracellular conductivity of cortical tissues and the cerebrospinal fluid can be as much as 6 to 10 (Nicholson and Rice, 1986). On the other hand, the extracellular conductivity of an anoxic region can be as little as 25% of that of a normoxic region (van Harreveld et al., 1965; Hansen and Olsen, 1980). According to Fig. 7, the magnetic field may be enhanced by 200% when the outer conductivity is 10 times the inner conductivity and reduced by as much as 90% when the ratio is reversed.

The ratio B_{sec}/B_{prim} for the different geometries (Figs. 7–9) indicates that the boundary effects should enhance the surface potential and magnetic field due to primary sources located in a tissue next to a region of higher conductivity (having a diameter >20 mm) and reduce those due to primary sources located in a tissue next to a region of lower conductivity. This result suggests that the external magnetic field and surface potential may be significantly enhanced when these signals are generated by neuronal sources next to a large edema or a region of the brain such as a temporal lobe that is removed for clinical reasons. On the other hand, these signals may be reduced when they are generated by primary sources next to an ischemic region, such as may occur during stroke, or a region of calcification.

Importantly, however, the above results indicate that the boundary effect should not be significant for the signals generated by cortical sources in one wall of a sulcus or a fissure in a normal brain. Cortical sources in sulci and fissures are dominant generators of the external magnetic field, since they are closest to the detectors. Also, functionally, these cortical sources are quite interesting in elucidating higher brain functions. The results in Fig. 9 indicate that the strong boundary effect of one sulcal wall should be cancelled by that of the opposite wall when they are separated by less than ~10 mm. The sulci and fissures in the normal brain are narrower than 5 mm (Gyldensted and Kostlejanetz, 1975) and, therefore, we expect that the external magnetic signal to be relatively free of the boundary effect in this case. The sulci in pathological cases (e.g., senile dementia and Alzheimer's disease), however, may be as wide as 10 mm (Huckman et al., 1975) and, therefore, the magnetic signals from the cortex of such patients may be enhanced compared with that of the normal, simply due to this anatomical difference.

The boundary effect should simply change the magnitude of the external magnetic field or surface potential without affecting their temporal waveforms if the primary source is stationary, i.e., if it does not move as a function of time. The enhancement or reduction of the overall magnitude of these signals should not cause serious difficulties in inferring functions of the brain, because their absolute magnitudes are usually not as important as their relative magnitudes. However, if the primary source does shift its location relative to a boundary, the temporal waveform of these external signals need not correspond exactly to the signals due solely to the primary source. This possibility should be especially real when the primary source is within ~0.5 mm of a highly conductive region such as the cerebrospinal fluid environment in a widened sulcus or a region filled with cerebrospinal fluid after removal of a tissue in surgery.

Although the boundary effects are exactly the same for the magnetic field and surface potential, these two signals are in general different (Okada, 1983; Okada et al., 1989). Examining Eq. 1, one sees that the potential on the scalp should be strongly influenced by the secondary sources just below the measurement position, namely those at the boundaries of the scalp, skull, and other interfaces. The moments of these secondary sources should be small relative to those near the primary source, but they should strongly influence the scalp potential because of their short distances to the measurement position. Also, small perturbations in the thickness of these layers can be magnified and distort the scalp potential. Unlike the electrical potential, the magnetic field is a vector quantity and thus it is possible to measure one of its components, namely the component normal to the scalp, that is less perturbed than the scalp potential. Because the secondary sources are directed normal to the boundary surface, the magnetic field due to the secondary sources at the scalp and skull should be parallel to their respective tangential plane of the boundary containing the secondary sources (Grynszpan and Geselowitz, 1973). Thus, the radial component of the magnetic field should be less affected by the secondary sources close to the measurement position than the scalp potential, even if one takes into account the nonspherical shape of the human head. The extracranial magnetic field should be less affected by the parameters such as conductivity and thickness of the scalp and skull, as compared to the scalp potential.

In sum, the present result shows that both the external magnetic field and surface potential may be significantly enhanced or reduced by the presence of abnormal regions in the brain such as an edema or an ischemic tissue or by the presence of a large ventricle as in the case of hydrocephalics and in various cases of cerebral atrophy (e.g., Alzheimer). The sulci and fissures, however, are not expected to significantly distort these signals in normal populations because they are narrower than 5 mm. The distortion should affect the scale factor of these signals when they are produced by stationary primary current generators. Their temporal waveforms, however, will be distorted when the generator shifts its location as a function of time.

APPENDIX

When a current dipole Q is located between two infinite parallel conducting plates separated by a distance $a + b$, a set of suitably placed image sources of appropriate magnitude can satisfy the required boundary conditions:

$$\Phi_{\text{in}} = \Phi_{\text{out}} \quad \text{and} \quad \sigma_{\text{in}} \frac{\partial \Phi_{\text{in}}}{\partial n} = \sigma_{\text{out}} \frac{\partial \Phi_{\text{out}}}{\partial n}. \tag{A1}$$

Suppose that the primary source is located at distance a from S_1 and at distance b from S_2 (cf. Fig. 3). These two surfaces produce pairs of images of the primary source along the axis of symmetry. Each pair of images are given by Eq. 2. The potential on S_1 due to the primary source in a homogeneous case ($\sigma_{\text{in}} = \sigma_{\text{out}}$) is given by Eq. 3 in the main text.

In inhomogenous cases, the potential on S_1 is given by the sum of the potential due to the primary source (Eq. 3) and those due to the images. There are two first-order image sources with respect to S_1 and S_2 which produce the following potential on S_1:

$$\Phi^{(1)}_{\text{image}} = -\frac{Q}{4\pi\sigma_{\text{in}}} \frac{\cos\theta}{a^2 + y^2 + z^2} \left(\frac{\sigma_{\text{out}} - \sigma_{\text{in}}}{\sigma_{\text{out}} + \sigma_{\text{in}}}\right) + \frac{Q}{4\pi\sigma_{\text{in}}} \frac{\cos\theta}{(2b + a)^2 + y^2 + z^2} \left(\frac{\sigma_{\text{out}} - \sigma_{\text{in}}}{\sigma_{\text{out}} + \sigma_{\text{in}}}\right), \tag{A2}$$

where y and z are the coordinates on the S_1 plane, θ is the angle between the current dipole and the position vector for the field point.

The potential on S_1 due to two second-order image sources is:

$$\Phi^{(2)}_{\text{image}} = -\frac{Q}{4\pi\sigma_{\text{in}}} \frac{\cos\theta}{(2b + a)^2 + y^2 + z^2} \left(\frac{\sigma_{\text{out}} - \sigma_{\text{in}}}{\sigma_{\text{out}} + \sigma_{\text{in}}}\right)^2 + \frac{Q}{4\pi\sigma_{\text{in}}} \frac{\cos\theta}{(2b + 3a)^2 + y^2 + z^2} \left(\frac{\sigma_{\text{out}} - \sigma_{\text{in}}}{\sigma_{\text{out}} + \sigma_{\text{in}}}\right)^2. \tag{A3}$$

In general, the potential on S_1 due to the pair of mth-order image sources can be found as:

$$\Phi^{(m)}_{\text{image}} = -\frac{Q}{4\pi\sigma_{\text{in}}} \frac{\cos\theta}{[(m - 1)b + ma]^2 + y^2 + z^2} \left(\frac{\sigma_{\text{out}} - \sigma_{\text{in}}}{\sigma_{\text{out}} + \sigma_{\text{in}}}\right)^m + \frac{Q}{4\pi\sigma_{\text{in}}} \frac{\cos\theta}{[(m + 1)b + ma]^2 + y^2 + z^2} \left(\frac{\sigma_{\text{out}} - \sigma_{\text{in}}}{\sigma_{\text{out}} + \sigma_{\text{in}}}\right)^m \tag{A4}$$

for $m = 1, 3, \ldots$, odd, and

$$\Phi^{(m)}_{\text{image}} = -\frac{Q}{4\pi\sigma_{\text{in}}} \frac{\cos\theta}{[mb + (m - 1)a]^2 + y^2 + z^2} \left(\frac{\sigma_{\text{out}} - \sigma_{\text{in}}}{\sigma_{\text{out}} + \sigma_{\text{in}}}\right)^m + \frac{Q}{4\pi\sigma_{\text{in}}} \frac{\cos\theta}{[mb + (m + 1)a]^2 + y^2 + z^2} \left(\frac{\sigma_{\text{out}} - \sigma_{\text{in}}}{\sigma_{\text{out}} + \sigma_{\text{in}}}\right)^m \tag{A5}$$

for $m = 2, 4, \ldots$, even. Thus, we have the representation of the total potential on surface S_1 (due to both primary source and images) as given by Eq. 4.

When $a = b$, which is when the primary source is in the middle of the slab, this equation can be reduced to:

$$\Phi = \frac{Q}{4\pi\bar{\sigma}} \sum_{n=0}^{\infty} \left(\frac{\Delta\sigma}{2\bar{\sigma}}\right)^{2n} \frac{\cos\theta}{[(4n + 1)a]^2 + y^2 + z^2} + \frac{Q}{4\pi\bar{\sigma}} \sum_{n=0}^{\infty} \left(\frac{\Delta\sigma}{2\bar{\sigma}}\right)^{2n-1} \frac{\cos\theta}{[(4n - 1)a]^2 + y^2 + z^2}. \tag{A6}$$

One can rewrite the dummy index $n = 2n$, and reduce the two summations as one series, as given by Eq. 5.

We thank Dr. N. Cuffin for helpful discussions.

This research was supported by NINDS grant R01-NS21149.

Received for publication 28 July 1989 and in final form 11 December 1989.

REFERENCES

Abramowitz, M., and I. A. Stegun. 1972. Handbook of Mathematical Functions. Dover Press, New York. 331–341.

Barnard, A. C. L., I. M. Duck, and M. S. Lynn. 1967*a*. The application of electromagnetic theory to electrocardiology. I. Derivation of the integral equations. *Biophys. J.* 7:443–462.

Barnard, A. C. L., I. M. Duck, M. S. Lynn, and W. P. Timlake. 1967*b*. The application of electromagnetic theory to electrocardiology. II. Numerical solution of the integral equations. *Biophys. J.* 7:463–491.

Barr, R. C., T. C. Pilkington, J. P. Boineau, and M. S. Spach. 1966. Determining surface potentials from current dipoles, with application to electrocardiography. *IEEE (Inst. Electr. Electron. Eng.) Trans. Biomed. Eng.* BME-13:88–92.

Berry, P. M. 1956. N, M space harmonics of the oblate spheroid. *Ann. NY Acad. Sci.* 65:1126–1134.

Cuffin, B. N. 1982. Effects of inhomogeneous regions on electric potentials and magnetic fields. *J. Appl. Phys.* 53:9192–9197.

Cuffin, B. N. 1985. Effects of fissures in the brain on electroencephalograms and magnetoencephalograms. *J. Appl. Phys.* 57:146–153.

Cuffin, B. N., and D. Cohen. 1977. Magnetic fields of a dipole in special volume conductor shapes, *IEEE (Inst. Electr. Electron. Eng.) Trans. Biomed. Eng.* BME-24:372–381.

Geselowitz, D. B. 1967. On bioelectric potentials in an inhomogeneous volume conductor. *Biophys. J.* 7:1–11.

Geselowitz, D. B. 1970. On the magnetic field generated outside an inhomogeneous volume conductor by internal current sources. *IEEE (Inst. Electr. Electron. Eng.) Trans. Mag.* MAG-6:346–347.

Grynszpan, F., and D. B. Geselowitz. 1973. Model studies for the magnetocardiogram. *Biophys. J.* 13:911–925.

Gyldensted, C., and M. Kosteljanetz. 1975. Measurements of the normal hemispheric sulci with computer tomography: a preliminary study on 44 adults. *Neuroradiology.* 10:147–149.

Hansen, A. J. 1985. Effect of anoxia on ion distribution in the brain. *Physiol. Rev.* 65:101–148.

Hansen, A. J., and C. E. Olsen. 1980. Brain extracellular space during spreading depression and ischemia. *Acta Physiol. Scand.* 108:355–365.

Hämäläinen, M. S., and J. Sarvas. 1987. Feasibility of the homogeneous head model in the interpretation of neuromagnetic fields. *Phys. Med. Biol.* 32:91–97.

Hämäläinen, M. S., and J. Sarvas. 1989. Realistic conductivity geometry model of the human head for interpretation of neuromagnetic data. *IEEE (Inst. Electr. Electron. Eng.) Trans. Biomed. Eng.* BME-36:165–171.

Huang, J.-C., Y. C. Okada, and C. Nicholson. 1989. Conductivity boundaries may produce stronger magnetic fields than the primary source: comparison of three analytical methods. Paper presented at the Seventh International Conference on Biomagnetism, New York. August 14–18.

Huckman, M. S., J. Fox, and J. Topel. 1975. The validity of criteria for the evaluation of cerebral atrophy by computed tomography. *Radiology.* 116:85–92.

Iramina, K., and S. Ueno. 1988. Spatial properties of magnetic fields produced by radially oriented dipole in inhomogeneous sphere. *In* K. Atsumi, M. Kotani, S. Ueno, T. Katila, S. J. Williamson, editors. Biomagnetism '87. Tokyo Denki University Press, Tokyo. 106–109.

Janday, B. S., and S. J. Swithenby. 1987. Analysis of magnetoencephalographic data using the homogeneous sphere model: empirical tests. *Phys. Med. Biol.* 32:105–113.

Lynn, M. S., and W. P. Timlake., 1968*a*. The numerical solution of singular integral equations of potency theory. *Numerische Mathematik.* 11:77–98.

Lynn, M. S., and W. P. Timlake. 1968*b*. The use of multiple deflations in the numerical solution of singular systems of equations, with applications to potential theory. SIAM (Soc. Ind. Appl. Math.) J. Numerical Anal. 5:303–322.

Meijs, J. W. H., H. B. K. Boom, M. J. Peters, and A. van Oosterom. 1987. Application of the Richardson extrapolation in simulation studies of EEGs. *Med. & Biol. Eng. & Comput.* 25:222–226.

Meijs, J. W. H., B. J. ten Voorde, M. J. Peters, C. S. Stok, and F. H. Lopes da Silva. 1988. The influence of various head models on EEGs and MEGs. *In* Functional Brain Imaging. G. Pfurtscheller and F. H. Lopes da Silva, editors. Springer-Verlag, Berlin, In press.

Nicholson, C., and M. E. Rice. 1986. The migration of substances in the neuronal microenvironment. Ann. NY Acad. Sci. 481:55–71.

Okada, Y. C. 1983. Neurogenesis of evoked magnetic fields. *In* Biomagnetism: An Interdisciplinary Approach. S. J. Williamson, G. L. Romani, L. Kaufmann, and I. Modena, editors. Plenum Press, New York. 399–468.

Okada, Y. C., M. Lauritzen, and C. Nicholson. 1987. Magnetic field associated with neural activities in an isolated cerebellum. *Brain Res.* 412:151–155.

Okada, Y. C., and C. Nicholson. 1988. Magnetic evoked field associated with transcortical currents in turtle cerebellum. *Biophys. J.* 53:723–731.

Okada, Y. C., C. Nicholson, and R. R. Llinas. 1989. Magnetoencephalography (MEG) as a new tool for non-invasive realtime analysis of normal and abnormal brain activity in humans. *In* Visualization of Brain Functions. Stockholm, Sweden. In press.

Smythe, W. R. 1968. Static and Dynamic Electricity. McGraw-Hill Book Co., New York.

Stok, C. J., J. W. H. Meijs, and M. J. Peters. 1987. Inverse solutions on MEG and EEG applied to volume conductor analysis. *Phys. Med. Biol.* 32:99–104.

Ueno, S., H. Wakisako, and S. Matsuoka. 1983. Determination of the spatial distribution of abnormal EEG and MEG from current dipole in inhomogeneous volume conductor. *Il Nuovo Cimento.* 2D:558–566.

Ueno, S., H. Wakisako, and K. Harada. 1985. Flux reversal phenomena in spatial distributions of the magnetoencephalograms. *In* Biomagnetism: Applications and Theory. H. Weinberg, G. Stroink, and T. Katila, editors. Pergamon Press, New York. 289–293.

van Harreveld, A., J. Crowell, and S. K. Malhotra. 1965. A study of extracellular space in central nervous tissue by freeze-substitution. *J. Cell. Biol.* 25:117–137.